ELSEVIER

Surface Science 418 (1998) 240–255

surface science

Silver films grown on a rhenium(0001) surface: a combined TDS, XPS, and $\Delta\Phi$ study

D. Schlatterbeck, M. Parschau, K. Christmann *

Institut für Physikalische und Theoretische Chemie der Freien Universität Berlin, D-14195 Berlin, Germany

Received 23 April 1998; accepted for publication 2 September 1998

Abstract

The energetics and kinetics of Ag thin film growth on Re(0001) were studied by means of temperature-programmed thermal desorption spectroscopy (TDS), X-ray photoelectron spectroscopy (XPS), and work function change ($\Delta\Phi$) measurements. The formation of three individual Ag layers shows up in TDS as three distinct desorption maxima β_1–β_3 appearing between 950 and 1010 K (β_3), between 900 and 960 K (β_2), and between 870 and 970 K (β_1). Except in the very low coverage (Θ) range, in which the desorption is a first-order process, the Ag desorption follows zero-order kinetics. For the first two layers, activation energy of desorption (E^*_{des}) is strongly Θ dependent: within the first layer, E^*_{des} increases almost linearly with Θ from $\approx$250 kJ mol^{-1} at Θ = 0.05 to about 290 kJ mol^{-1}, reflecting attractive Ag–Ag interactions. From Θ = 0.5 to 0.9, E^*_{des} rises by only some 10 kJ mol^{-1}. A similar (but much less pronounced) Θ dependence appears for the second monolayer. A detailed shape analysis of the submonolayer TD spectra reveals a phase equilibrium between Ag condensed in islands and individual, mobile Ag atoms (2D gas phase). In XPS, the absence of any energy shift of the Ag and Re core levels underlines the weakness of chemical Ag–Re interactions. Two Ag layers lower the work function of the Re(0001) surface by about 750 meV, with a shallow minimum near the second monolayer. We discuss our data in conjunction with previous STM and LEED results for the same system and compare this system with other Ag-on-metal systems.

Keywords: Rhenium; Silver; Single crystal surfaces; Single crystal epitaxy; Photoelectron spectroscopy; Thermal desorption spectroscopy; Work function measurements; Epitaxy; Evaporation and sublimation; Growth; Thermal desorption; Metal–metal interfaces; Metal–metal nonmagnetic thin film structures

1. Introduction

In recent years, metallic thin films have received increasing interest in chemistry and physics owing to their role in such applications as industrial catalysis, materials science, optics, and energy technology [1,2]. The use of metallic films in heterogeneous catalysis deserves particular attention, because their chemical properties are often significantly modified by the support material (which may consist either of insulators such as alumina, silica or zeolites, or of metals and alloys/intermetallic compounds). In this respect, the metals Au and Ag which are catalytically not too active in their compact form, can become quite reactive if they are deposited on a support material in a highly dispersed form. This has been shown, e.g., for the CO oxidation over Au/TiO_2 by Haruta [3] and for selective hydrogenation reactions over Au or Ag/SiO_2 by Claus [4].

Apart from this "chemical" influence, the sub-

* Corresponding author. Fax: +49 30 8384792;
e-mail: kchr@chemie.fu-berlin.de

0039-6028/98/$ – see front matter
PII: S0039-6028(98)00719-5

strate can crucially govern the morphology of the deposit – its growth and geometric structure depend sensitively on the orientation of the host crystal (“epitaxy”), and pseudomorphism of the first layer(s) of the deposit is often observed. Quite generally, the growth features simply reflect the interplay between the energetics (thermodynamics) and kinetics of the interacting system. This interplay is largely determined by the thermal energy (temperature) of the system. The link to surface chemistry is provided by the fact that structure and degree of dispersion of a given (bi)metallic film will markedly affect its chemical reactivity. In previous LEED and STM work [5] we examined the morphology of the Ag/Re(0001) system. We showed that the first Ag layer grew pseudomorphically, followed by a uniaxially expanded second layer, until Ag(111) crystallites formed in a pseudo Frank–van der Merwe mechanism, with an intermediate quasi-hexagonal coincidence structure caused by misfit-dislocation domains. This growth behavior, along with the high mobility of the Ag atoms on the Re surface, suggested a minor “chemical” interaction between the two metals. This could be expected from their similar Pauling electronegativities and from the fact that they do not form alloys in the bulk [6].

In the present work, we supplement combined TDS, XPS, and $\Delta\Phi$ data on the Ag/Re(0001) system to correlate and understand the energetics and kinetics accompanying the growth of the Ag layers on the Re(0001) surface. Where necessary, we will compare and correlate the previous STM data with the results of this work.

Surfaces of the hcp metals Ru and Re have frequently been used as substrates for thin film deposition [7–17]. Their high melting point provides a convenient possibility for thermal desorption of the deposited material by monitoring the metal’s vapor pressure mass spectrometrically. We refer especially to Bauer’s pioneering work on noble metal deposition onto W or Mo surfaces [18–29]. Combined LEED, AES, TDS, and $\Delta\Phi$ measurements have helped to characterize not only the kinetics and energetics, but also the surface geometric and electronic structure and the growth of the thin films. Based on the Polanyi–Wigner equation [30], Bauer and coworkers developed a powerful data evaluation procedure which allowed the determination of (coverage-dependent) frequency factors ν, desorption activation energies E^*, and reaction orders x from a lineshape analysis of TD spectra [18,19]. An equivalent lineshape analysis to derive ν, E^*, and x as a function of the deposit concentration was suggested by King [31]. (We shall return to the details of these data evaluation procedures in Section 3.) As far as thin film studies on the basal hcp metal surfaces of Ru and Re are concerned, we mention our own work [5] and reports by Behm et al. [10–13] and Wandelt et al. [9,16]. Furthermore, we refer to a comprehensive review by Campbell [32] surveying both structural properties and chemical reactivities of the thin films as probed by gas adsorption and surface reactivity. Extensive studies of the Cu/Re(0001) system by Rodriguez et al. [33] and by He and Goodman [34,35] also deserve attention.

2. Experimental

Thin silver films on Re(0001) were prepared as described previously [5], though in a different UHV system. The vacuum chamber contained facilities for Auger electron spectroscopy (AES), thermal desorption spectroscopy (TDS), low-energy electron diffraction (LEED), X-ray photoemission spectroscopy (XPS), and work function change ($\Delta\Phi$) measurements. Vacuum was maintained by means of a $400\,l\,s^{-1}$ ion getter pump, a $240\,l\,s^{-1}$ turbomolecular pump, and a mechanical roughing pump. After appropriate bake-out, the chamber background pressure was about 8×10^{-11} mbar; during deposition of Ag, it never rose beyond 5×10^{-10} mbar.

The sample consisted of a disk-shaped Re(0001) crystal of 5 N purity (diameter $\approx$ 8 mm, thickness $\approx$ 1 mm), X-ray oriented to within 0.5°. After careful mechanical polishing to a mirror-like finish it was mounted on a standard sample manipulator. Sample heating could be performed by electron bombardment ($T_{max}\approx2500$ K) or by passing a direct current through the Ta support wires, with temperatures being measured using a W/WRe thermocouple (W97Re3/W75Re25) spot-welded

to the side of the crystal. Temperatures were controlled by a PID regulator which could be operated either manually or by a computer and provided linear heating ramps. Cleaning of the surface was attained by a few minutes heating in oxygen ($P_{O_2} \approx 2 \times 10^{-8}$ mbar) at $T = 1100$ K, followed by a short heating to 1500 K in a hydrogen atmosphere ($P_{H_2} \approx 10^{-7}$ mbar) and a final flash to 2300 K in order to remove residual oxygen. Excessive Ar ion sputtering was avoided in order keep damage to the surface to a minimum. The cleaning procedure was extended until AES revealed the complete removal of sulfur, carbon, and oxygen contaminants and the LEED pattern showed bright and sharp diffraction spots indicative of a clean, well-annealed hcp(0001) surface.

Deposition of Ag was accomplished using a commercial Knudsen cell (WA technology) loaded with ultrapure Ag wire (Goodfellow, 99,99% purity); temperatures at the cell could be kept constant to within 1 K resulting in very constant, reproducible deposition rates. A quartz microbalance (Balzers) allowed precise control and calibration of the flux of Ag atoms. Deposition rates could thus be varied between 0.1 an 1.1 ML min^{-1}. Highly reproducible TPD data were obtained by a screen with an aperture of 3 mm $\varnothing$ which could be placed between the Knudsen source and the sample (diameter $\approx$ 10 mm) as well as between the sample and the quadrupole mass spectrometer (Balzers, QMG 112A).

For XPS, we used a double-anode X-ray source providing Al Kα radiation (Leybold, RQ-20/38B). The emitted photoelectrons were analyzed with respect to their kinetic energy by means of a spherical electron energy analyzer (VG, Clam II). providing a resolution of $\approx$200 meV. The same analyzer was also used for AES, whereby a standard electron gun served as a source for primary electrons. The gun was operated with beam currents less than 5 mA in order to avoid thermal damage on the Ag thin films.

Work functions and work function changes were followed by means of a (home-made) Kelvin probe with an inert Ta wire electrode. Because of the geometry, variations of the work function during Ag deposition could not be monitored continuously, but only after each deposition. This discontinuous measurement required a frequent readjustment of the Kelvin capacitor and limited the $\Delta\Phi$ resolution to approximately $\pm$20 meV.

The as-deposited Ag films were very clean as monitored by XPS and LEED. The condensed amounts ("Ag coverages" Θ) could be conveniently estimated from (i) the frequency shift of the quartz microbalance, (ii) the area of the Ag $3d_{5/2}$ and $3d_{3/2}$ XPS signal between 360 and 380 eV electron energy, and (iii) the Ag TDS peak integrals. As will be shown below, the determination of absolute Ag coverages must take the appreciable lattice misfit between fcc Ag and hcp Re into account: the closest Ag–Ag distance in the bulk is $d_{Ag} = 2.884$ Å, while $d_{Re} = 2.761$ Å, resulting in a positive lattice misfit of $\approx$4.6%.

We define an absolute silver coverage in the usual way, namely, as the number ratio between the first-layer Ag atoms and surface atoms of the Re(0001) crystal. $\Theta_{Ag} = 1$ then means 1.515×10^{19} m^{-2}. Note, however, that our previous STM investigation revealed that Ag grows pseudomorphically only in the first layer, forming coincidence structures for the second and third layers, and finally, after six layers, Ag(111)-oriented crystallites [5]. Accordingly, the number of Ag atoms per layer decreases slightly as one moves away from the Re(0001) surface towards the Ag(111) crystal, and there arises a small, but noticeable, layer dependence of the Ag layer filling: if we associate the pseudomorphic first Ag layer with the absolute coverage $\Theta = 1$ all layers beyond the third merely contain 1.388×10^{19} atoms m^{-1}, which corresponds to $\Theta = 0.91$. The aforementioned lattice misfit is responsible for (temperature-dependent) strain effects in the first and second layer which affect the growth behavior and energetics: room temperature Ag deposits – in the following called RT films – cause a largely dendritic shape of the islands; even near the monolayer the films have many pores, and there occurs an incomplete layer-by-layer growth. However, if the Ag is deposited at higher temperatures (HT films), the edges of the nuclei and islands are much less fringed, and the first two monolayers exhibit fewer defects and pores. In the multilayer regime, up to three incomplete Ag layers still coexist, resulting

in an "incomplete" Frank–van der Merwe growth mechanism [5].

A decisive quantity throughout our experiments is the flux of Ag atoms emitted from the Knudsen cell. To check the constancy of the Ag flux, Ag was deposited onto the substrate for different time intervals before desorption spectra were taken. The actual surface coverage can easily be obtained from an integration of these spectra, $\int P_{Ag}\,dt$. The observed, absolutely linear, relationship between $\int P_{Ag}\,dt$ and time t demonstrates that two important conditions are fulfilled: (i) the Knudsen cell provides indeed a very constant flux of Ag atoms, and (ii) the condensation coefficient of Ag on Re(0001) is likewise constant, i.e. does not depend on coverage, at least not in the temperature range investigated.

3. Results

3.1. Thermal desorption spectroscopy

The Re(0001) surface was kept at a constant temperature (mostly ≈ 740 K) and exposed, for different time intervals, to distinct fluxes of Ag atoms (ca. 1.2 monolayer (ML) per minute), the background pressure being $\approx 5 \times 10^{-10}$ mbar. The TD data were recorded by a multichannel 16 bit AD converter. The desorption experiments were performed at heating rates ($\beta = dT/dt$) between 1 and 7 K s^{-1}, but mostly at $\beta = 2.5$ K s^{-1}, which yielded the best thermal resolution of the TD peaks. In some cases, we chose a somewhat higher value for β (5 or 7 K s^{-1}) in order to improve the signal-to-noise ratio. At substrate temperatures of 740 K the deposited Ag atoms have sufficient mobility to reach their equilibrium sites and form, if possible, structures with long-range order. To rule out any losses of Ag atoms prior to a desorption experiment we systematically varied the sample temperature between 600 and 750 K during deposition, but both the shape and the intensity of the spectra remained unaffected.

Fig. 1 displays three series of TD spectra reflecting different final Ag coverages. Fig. 1a shows a series spanning the coverage range from 0 to ca. 2 Ag monolayers (ML), with a coverage increment

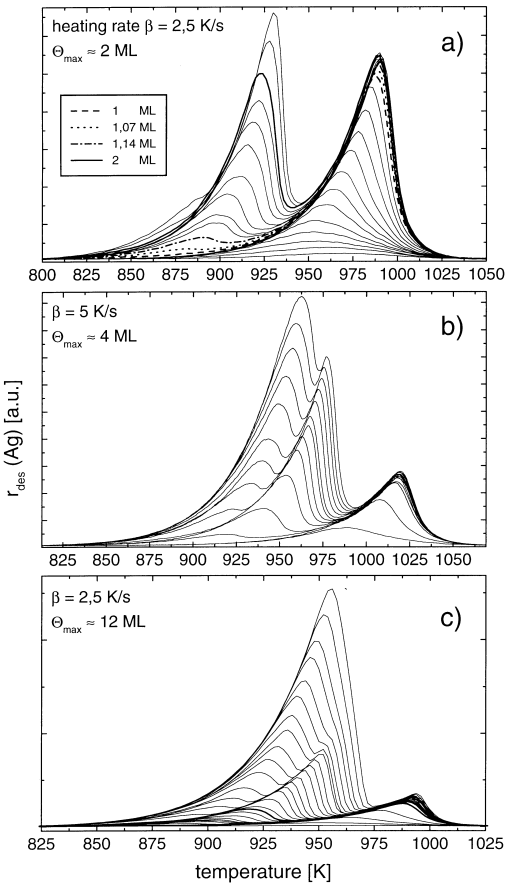

Fig. 1. Three series of thermal desorption spectra with different initial coverages Θ_0: (a) $\Theta_0 \approx 2$ ML, heating rate $\beta = 2.5$ K s^{-1}; (b) $\Theta_0 = 4$ ML, $\beta = 5$ K s^{-1}; (c) $\Theta_0 = 12$ ML, $\beta = 2.5$ K s^{-1}. The TD curves reflecting full monolayer populations are drawn in bold. See text for further details.

of about 0.1 ML from spectrum to spectrum. Obviously the growth of Ag takes place layer by layer. However, the growth of the second layer sets in before the first monolayer is really completed (see below). It is apparent even at a first glance that the order of the desorption reaction, for both layers, changes with coverage. For medium and high coverages the TD spectra exhibit a common leading edge, indicative of a zero-order desorption kinetics. Clearly, the desorption maxima fall almost together with the exponentially rising rate curve and vary, therefore, strongly with coverage. By contrast, below $\Theta \approx 0.2$, the TD maxima first appear at some 10 K higher temper-

atures and shift, in an apparent second-order fashion, to higher temperatures as the coverage decreases. Certainly, there is no true second-order process involved, since no Ag dimers appear in the mass spectrum. Instead, we regard this effect as a consequence of the application of the Polanyi–Wigner equation

$$\text{rate} \equiv -\frac{\mathrm{d}\Theta}{\mathrm{d}t} = \nu(\Theta)\Theta^{x} \exp\left(\frac{E^{*}_{\mathrm{des}}(\Theta)}{kT}\right) \qquad (1)$$

which arises solely from a superposition of first- and zero-order rate processes in a limited Θ interval, for constant E^{*}_{des} and ν. This view is supported by a simulation of our TD spectra which is further explained in Section 4. A convenient way to follow the Θ dependence of the order of the desorption kinetics is provided by so-called order plots [36,37]. Their construction is based on the validity of Eq. (1) and consists of a double-logarithmic plot of the desorption rate against coverage for various temperatures. In a sense, the curves obtained are "isotherms" of the desorption rate; their slope reflects the order x. Fig. 2 shows the order-plot representation for the TD spectra of Fig. 1a. For the coverage ranges $0.2<\Theta<0.86$ and $1.2<\Theta<1.7$ they reveal horizontal lines, i.e., $x=0$, whereas for low coverages within the first and second monolayer the slope (and, hence, x) is 1. Difficulties in the interpretation arise for a low Θ regime between the first and second layer ($0.8<\Theta<1.1$). Owing to the strong variation of E^{*}_{des} in this range the order plot yields invalid results [38].

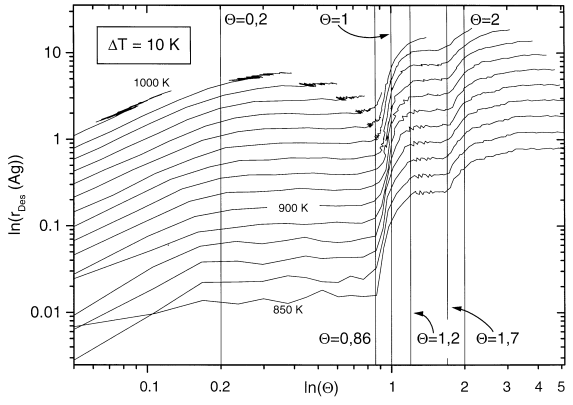

Fig. 2. "Order plot" for Ag desorption from Re(0001). In the coverage ranges $0.15<\Theta<0.86$ and $1.2<\Theta<1.7$ the slope of the desorption rate isotherms (and therefore the desorption order) is zero. At low coverages within the first and second monolayer, the desorption follows a first-order kinetics. For $0.86<\Theta<1$ the desorption energy changes markedly which renders the interpretation of the slope meaningless [38].

Returning to the "ordinary" TPD spectra, we refer to Fig. 1b which displays higher integral Ag coverages up to 4 ML (this set of spectra was measured with a higher $\beta=5\ \mathrm{K\ s^{-1}}$) and shows quite clearly the common leading edge associated with the desorption peak of the second layer. Furthermore, the desorptive contributions of the individual layers are no longer resolved, i.e. a distinction between the third, fourth, fifth layer etc. is no longer possible. Instead, the multilayer TD peak grows continuously and finally follows a genuine zero-order desorption kinetics. This situation is emphasized in Fig. 1c which spans a maximum Ag coverage of 12 ML.

Although the TD spectra contain in principle all information about the "state" of the interacting Ag and Re species, it is not quite easily accessible. Various procedures providing access to the physical properties have thus been described in the literature, most of them departing from the Polanyi–Wigner equation (Eq. (1)). In a first-hand evaluation we may assume strict zero-order kinetics ($x=0$) for all desorption processes. Besides negligible readsorption of Ag (a condition fulfilled in metal desorption experiments) this assumption rests on a single, Θ-independent, binding state for each layer with layer-specific, but constant, values of E^{*}_{des} and ν. Our TD spectra suggest that this assumption is valid already for the medium and higher coverage ranges of the first and second monolayer, as well as for desorption from multilayers. This latter process is entirely equivalent to a sublimation of Ag, so that one expects a single exponential rate law for desorption from each layer. The respective Arrhenius plots, namely ln(rate) versus reciprocal temperature, yield indeed reasonably straight lines for all three discernable TD states, cf. Fig. 3. We obtain $E^{*}_{\mathrm{des}} \approx 293.2\ (\pm 4)$ kJ mol^{-1} for the first-layer Ag, 273.3 (± 5) kJ mol^{-1} for the second layer, and 273.5 (± 5) kJ mol^{-1} for desorption from the Ag multilayer. This final value agrees very well with the heat of

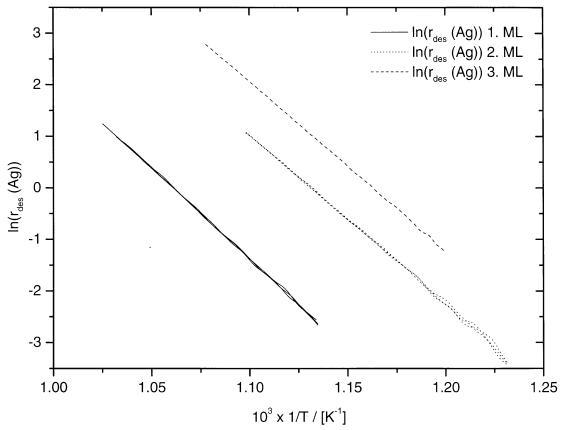

Fig. 3. "Arrhenius-type" plots, i.e. ln(desorption rate) versus reciprocal temperature. For an approximately zero-order process, the three TD states of Fig. 1c yield reasonably straight lines which allow the determination of the activation energy for desorption. One obtains $E^{*}_{\mathrm{des}} \approx 293.2\ (\pm 4)$ kJ mol^{-1} for the first Ag layer (top curve), 273.3 (± 5) kJ mol^{-1} for the second layer (middle curve), and 273.5 (± 5) kJ mol^{-1} for desorption from the multilayer (bottom curve).

sublimation of silver, ΔH_{sub}, which is given in Ref. [39] as 270 kJ mol^{-1}.

Before we turn to the determination of coverage-dependent activation energies and frequency factors by means of a complete analysis it is necessary to return to the problem of evaluating actual (absolute) Ag coverages Θ_{Ag}. In Fig. 1, the first desorption maximum could be associated with the filling of the first monolayer, giving us at least a relative measure of the monolayer population. Since Ag grows pseudomorphically in the first layer [5], we may state an absolute number for the Ag monolayer concentration, namely, 1.515×10^{19} m. This number requires a perfect order of all Ag atoms, which is, however, a largely idealized assumption in view of the relatively open morphology of the first layer suggested by the STM images [5]. We therefore regard these absolute numbers as an upper limit for Θ; the real coverages may be 5 or 10% lower. If we extend the concentration of the Ag deposit well into the multilayer regime, there remains the task to determine the monolayer filling and the onset of the second-layer growth.

A very elegant way to obtain this information has recently been proposed by Schlichting and Menzel [40]. It is based on the construction of so-called layer plots. For this construction, the ordinary TD spectra (shown, for example, in Fig. 1) are integrated from left to right. For each desorption rate (= ordinate) one obtains the residual coverage

$$\Theta_{\mathrm{res}} = \int_{t \triangleq T}^{t=\infty} P_{\mathrm{Ag}}\, \mathrm{d}t.$$

Then the desorption rate is plotted against Θ (which is high at low temperatures T and vanishes at sufficiently high T). The initial coverage Θ (prior to the application of the temperature program) of each spectrum follows from the intercept. Accordingly, in this layer plot the temperature increases from right to left, although it no longer explicitly appears in the spectra as a variable. Hence, the common TD spectra are inverted from left to right, and one should actually "read" a layer plot from right to left. The sequence of TD maxima appears in the layer plots in a more pronounced way than in the conventional TD spectra, and one can easily associate the various maxima with the layer-specific desorptive contributions. For well-separated TD maxima there are deep "valleys" in the layer plots whenever the population of an individual layer becomes exhausted (resulting in a sharp drop of the desorption rate). Slightly higher temperatures remove the material of the next layer underneath so that the desorption rate rises again, and so forth. Thus, the various layers can be well distinguished from one another.

Fig. 4 displays the layer-plot representation of some of the TD curves of Fig. 1b (the thin perpendicular lines are explained below). The aforementioned "valleys" in the layer plot allow the accurate determination of the monolayer coverages. However, a careful inspection of the minimum between the first, second, and third layers reveals a slight shift of the minimum towards smaller residual coverages as the overall Ag coverage increases from the monolayer into the multilayer range. Interestingly, the extent of this shift – which is a direct measure of the population of Ag atoms within the first layer – depends on how much material is contained in the second layer. This is

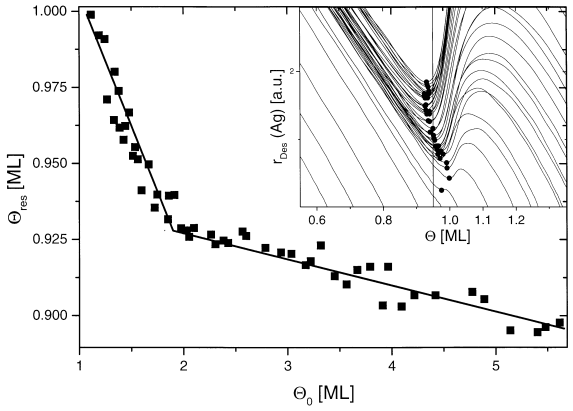

Fig. 4. "Layer" plots of some of the TD spectra shown in Fig. 1b. For their construction, the "ordinary" TD spectra are integrated from left to right to yield the residual coverage $\int_{t\triangleq T}^{t=\infty} P_{\mathrm{Ag}}\,\mathrm{d}t = \Theta_{\mathrm{res}}$, before the desorption rate is plotted against Θ_{res}. Absolute coverage calibration is provided by the minimum between the contributions from the first and second layer. The thin perpendicular lines indicate the nominal Ag monolayer coverages. See text for the details.

illustrated by means of Fig. 5 which displays the residual coverage of the first monolayer (in an enlarged scale) as a function of the initial Ag coverage prior to the desorption experiment (for the scaling of the axes in ML units, see below). Fig. 5 reveals two clear linear sections that separate the first "bilayer" from all subsequent Ag layers, thus demonstrating that the content of Ag atoms of just the first layer is strongly affected by the population of the second layer in such a way that a greater filling of the second layer reduces the Ag content of the first layer. This behavior indicates that the maximum number of first-layer atoms and, hence, the morphological stability of the first layer is not independent of the second-layer population. We will return to this point in Section 4.

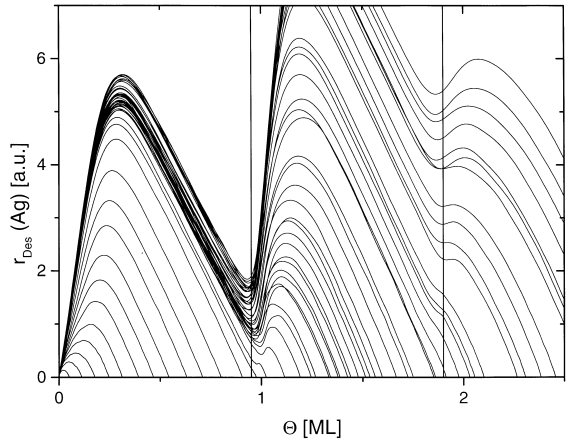

Fig. 5. Plot of the residual coverage Θ_{res} of the first monolayer against the initial Ag coverage, i.e. prior to the desorption experiment. The figure reveals two clear linear sections which separate the first "bilayer" from all subsequent Ag layers, thus demonstrating that the populations of the first and second Ag monolayer are not independent of each other. The inset shows a magnification of the minimum occurring in the Ag desorption rate between the first- and second-layer contribution, cf. Fig. 4.

The absolute coverage calibration was carried out using the layer plots of Fig. 4. The minimum which separates the desorptive contributions of the first and second layer is enlarged in the inset to Fig. 5. The trace corresponding to an initial coverage of $\Theta = 1.1$ exhibits the minimum at the highest residual coverage Θ_{res}, i.e. it marks the point on the coverage scale with the maximum amount of Ag present in the pseudomorphic first monolayer. Therefore, we assign this particular coverage as $\Theta \equiv 1$ (substrate units). However, since the pseudomorphic growth is restricted to the first monolayer only, this Θ calibration also holds for the first monolayer only. (In the second and third Ag layer, the monolayer Ag content is somewhat smaller.)

In order to derive (coverage-dependent) activation energies for desorption, frequency factors, and reaction orders, two (quite similar and entirely equivalent) TD data analyses have been suggested and successfully applied for various metal-on-metal and gas-on-metal interaction systems [18,41]. Both make use of the (Θ-dependent) Polanyi–Wigner equation. We applied both analyses to our sets of data and obtained identical results. We will therefore focus here only on Bauer's procedure [18]. The thermal desorption is expressed in terms of a residence time τ of the individual particle on the surface, as given by the equation:

$$\tau \equiv -\frac{\Theta}{\mathrm{d}\Theta/\mathrm{d}t} = \frac{1}{\nu(\Theta)\Theta^{x-1}} \exp\left(\frac{E^{*}_{\mathrm{des}}(\Theta)}{kT}\right) \qquad (2)$$

The TD spectra are then integrated with respect to small T intervals, and, for a given temper-

ature, one obtains the residual coverage $\Theta_{res} = \int_T^{\infty} d\Theta/dt$, while the rate is given by the respective ordinate at $T + dT$. More details of the evaluation procedure can be found in the original work [18]. This analysis allows us to determine both the frequency factor ν and the activation energy of desorption E^*_{des} as a function of Ag coverage. For the first monolayer, both relations, $\nu(\Theta)$, upper graph, and $E^*(\Theta)$, bottom panel, are shown in Fig. 6. Note that the evaluation of E_{des} does not depend on an assumption for the reaction order x, while the determination of ν makes sense only if x is independent of Θ. However, since x changes with Θ at medium coverages from values around 1 to 0, the Θ dependence of ν presented in the following is only qualitatively correct.

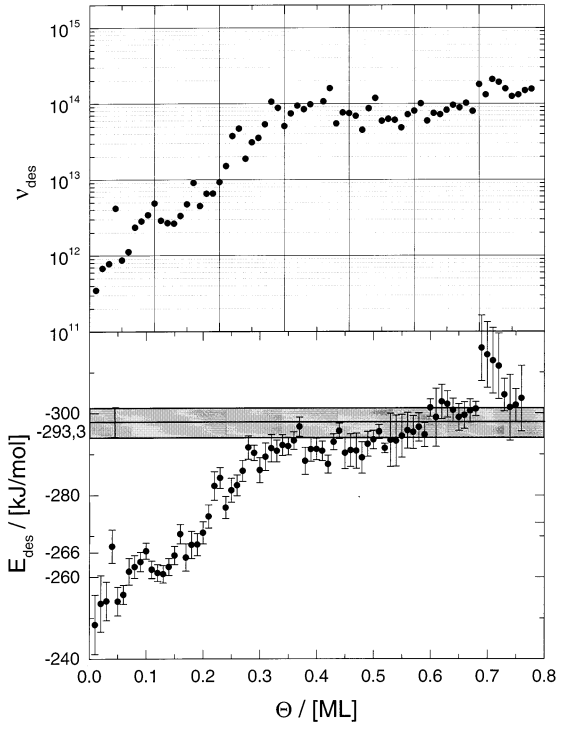

Fig. 6. Result of the line-shape analysis according to Bauer et al. [18], which was applied to the series of Ag TD spectra shown in Fig. 1a for the coverage range $0 < \Theta < 1$ ML. Upper panel, frequency factor ν; lower panel, activation energy of desorption E^*_{des} as a function of Ag coverage. At low Θ, $E^*_{des} = 250$ kJ mol^{-1}; for $\Theta > 0.3$ to 0.4, $E^*_{des} \approx 290$ kJ mol^{-1}. Also indicated in the figure is the result of the simple zero-order analysis as a bold horizontal line.

For both functions, $E^*_{des}(\Theta)$ and $\nu(\Theta)$, we find an absolute parallel Θ dependence (which may indicate a pronounced compensation effect [42]). At low coverages, the activation energy for desorption is quite small, namely 250 kJ mol^{-1}, and increases almost linearly with coverage, until around $\Theta \approx 0.3$ to 0.4 a practically constant value of 290 kJ mol^{-1} is reached. Quite close to the filling of the monolayer there occurs a sharp drop of E^*_{des} (which is well known to occur with metal desorption [24,25] and is partially attributed to the data evaluation procedure, see below). All in all, the data we obtain for the activation energy of desorption at medium and high coverages agree quite well with the result of the simple data analysis which rested on a zero-order rate process and coverage-independent E^*_{des}. The frequency factor ν is around 5×10^{11} s^{-1} near zero coverage and increases to values around 10^{14} s^{-1} at medium and high coverages, compatible with immobilized layers.

However, the apparent deviations from zero-order desorption kinetics in the submonolayer regime ($0 < \Theta < 0.2$) call for a more sophisticated data evaluation procedure based on fundamental statistical mechanics. Such an analysis has been carried out and will be described in a separate paper [43]. An important result of this evaluation is the apparent change of the reaction order which can be entirely understood assuming a 2D gas-phase→2D solid transition in which "solid" 2D islands with immobile Ag atoms are in equilibrium with "gaseous", mobile, Ag atoms. It is well feasible that an Ag atom must first dissolve from the 2D solid and transform to the 2D gas phase before it can desorb. This phenomenon of phase separation has previously been described in the literature on metal desorption [23,44].

Another problem arises if the data analysis procedure described above is applied to the TD spectra for $\Theta > 1$ ML. In order to obtain genuine information on the TD peak shape of the second layer, the first-layer contribution must be subtracted from the integral signal. This requires that the peaks are sufficiently separated. In our evaluation, we subtracted the "artificial" monolayer spectrum (see above) from all spectra that contained a second-layer contribution. However,

since – for reasons pointed out above – the absolute coverage for the first layer varies somewhat with the second-layer population ($\Theta = 1$) this difference is sensitively affected, if the population of the second layer is still low or already quite high. Therefore, we had to cut off the high-temperature tail from the spectra after subtraction. Furthermore, it should be kept in mind that some Ag atoms will change from the first to the second or from the second to the third layer and vice versa during desorption, so that one should not overinterpret the E^*_{des} and ν data near the filling of a complete monolayer ($0.86 < \Theta < 1.1$ and $\Theta > 1.7$). This Θ range was therefore omitted from Figs. 6 and 7.

The resulting Θ dependence of the second monolayer is illustrated in Fig. 7. It resembles somewhat the course of $E^*_{des}(\Theta)$ for the first monolayer, i.e. it shows a first slight increase from 250 to ≈ 275 kJ mol^{-1} at medium coverages, where it remains practically constant, until it decreases slightly near the completion of the layer. The frequency factor, in turn, increases from 10^{12} to 10^{14} s^{-1} in the same Θ range.

The TD spectra of Fig. 1 clearly show that a fourth or fifth desorption peak can no longer be separated from the third one, demonstrating that energetic differences between the Ag atoms bound in the respective layers are so small that desorption from several layers can occur simultaneously and a single rate equation is no longer a valid description of the desorption process. Accordingly, for the third and all subsequent layers our analyses yield values close to the heat of sublimation of bulk silver, ΔH_{sub}, as characteristic for metal-on-metal desorption experiments.

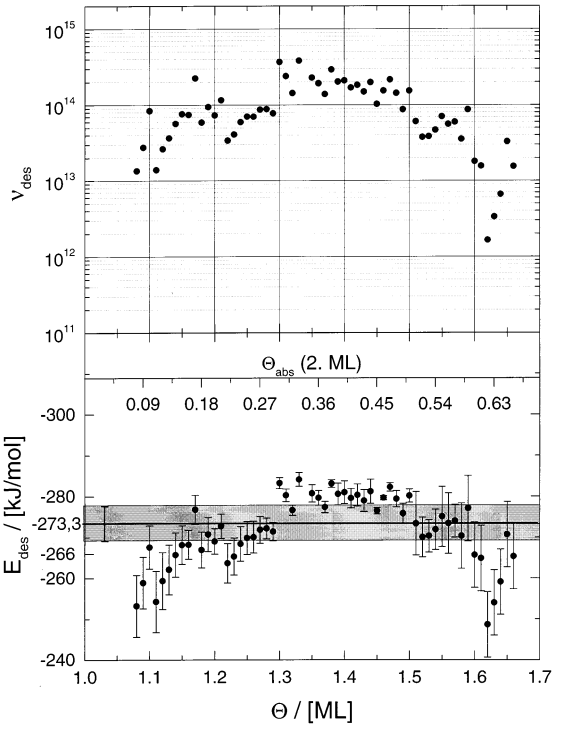

Fig. 7. Same representation as Fig. 6, but for the second Ag monolayer. Upper panel, frequency factor ν; lower panel, activation energy of desorption E^*_{des} as a function of Ag coverage (within the second monolayer). Again at low Θ, $E^*_{des} = 250$ kJ mol^{-1}; for $\Theta > 1.3$, E^*_{des} reaches 280 kJ mol^{-1}, but decreases again for $\Theta > 1.5$. The result of the zero-order evaluation ($\rightarrow E^*_{des} = 273.3$ kJ mol^{-1}) is practically identical to the heat of sublimation of bulk Ag, i.e. $\Delta H_{sub} = 275$ kJ mol^{-1}.

3.2. X-ray photoelectron spectroscopy (XPS)

Most of our XPS data were obtained with unannealed Ag films deposited at room temperature at a rate of ≈ 1.3 ML s^{-1}. Some control measurements were also performed with HT films in order to investigate alloying effects that could possibly occur at elevated temperatures. However, no differences between RT and HT films could be detected. This statement is valid both for the signal intensity – coverage dependence and for the energetic positions of the various Re and Ag core levels.

Fig. 8 shows two sets of (Θ-dependent) XP spectra obtained from RT films. Fig. 8a displays four complete spectra including the clean Re surface and a 10 Ag ML film and gives an impression of the relative peak intensities of the spin–orbit-split d core levels. Fig. 8b contains the spectra of the energy ranges of the Re $4d_{5/2}$ and $4d_{3/2}$ levels (250–300 eV) and the Ag $3d_{5/2}$ and $3d_{5/2}$ levels (360–390 eV). 18 spectra are presented, with the Ag coverage varying in 0.2 ML steps up to 4.0 ML. It can be seen that there occurs – within the limits of accuracy – no core level binding energy shift, neither of the Re nor of the Ag electron energy levels. This absence of a chemical shift supports

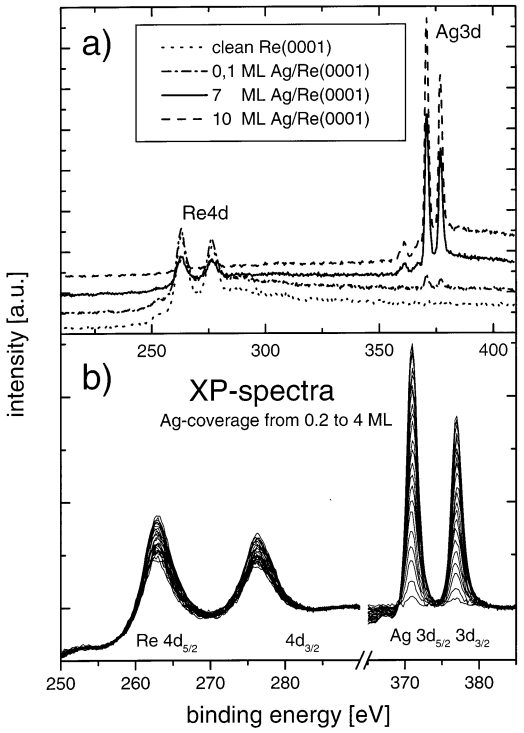

Fig. 8. Two sets of (coverage-dependent) XP spectra obtained from Ag films deposited at 300 K. (a) Four complete spectra including the clean Re surface and a 10 Ag ML spectrum and showing the spin–orbit-split doublet of the Re 4d and the Ag 3d core level excitation. Note the absence of any core-level shifts in both Re and Ag signals. (b) Series of XP spectra, obtained under the same conditions as in (a), but displaying the energy range in which the Re $4d_{5/2}$ and $4d_{3/2}$ levels (250–300 eV) and the Ag $3d_{5/2}$ and $3d_{3/2}$ levels (360–390 eV) are visible. Altogether 18 spectra are shown, with the Ag coverage varying in 0.2 ML steps up to 4.0 ML. Again, there are no core level shifts recognizable.

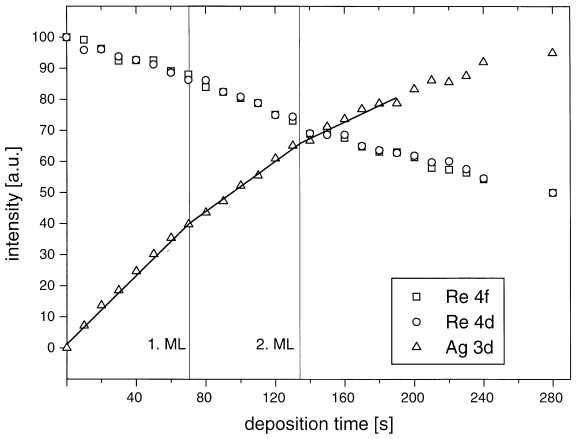

Fig. 9. Integrated peak areas for both Re and Ag XP signals (Re 4f and 4d, and Ag 3d orbital excitations) as a function of deposition time under constant flux and temperature conditions. Thin vertical lines mark the deposition times at which, according to the TD spectra of Fig. 1, the individual monolayers are filled. Especially in the Ag signal, two clear breaks in the slope support our layer calibration and suggest a layer-by-layer growth mode.

our suggestion made above that the chemical interaction between Ag and Re is weak. This point will be taken up again in Section 4.

In Fig. 9 we plot the respective peak areas for both Re and Ag as a function of deposition time under constant flux and temperature conditions. Thin vertical lines indicate the deposition times at which the completion of individual monolayers is expected from the thermal desorption experiments. Especially the Ag XPS signal intensities exhibit fairly abrupt distinguishable changes of the slopes coinciding with the expected fillings of the monolayers. Not only does this behavior confirm our TDS coverage calibration, but it allows us in addition to determine the inelastic mean free path (λ_{imfp}) of the ejected (kinetic energy ≈ 300 eV) photoelectrons. We may take the λ_{imfp} data suggested by Tanuma et al. [45] (presented in Table 1) as a reference. In our XP spectra of the 10 ML Ag film, the Re photoelectrons possess merely $\approx 14\%$ of their intensity of the clean Re. Using the data of Table 1 and assuming a 10 ML film with a thickness of ≈ 25 Å, the Re electron intensity should have become damped to about 12% of the initial value. The good agreement with the calculated value supports the idea of a layer growth of the Ag. The other, even more relevant, information accessible from Fig. 9 concerns the growth mode of the Ag deposit on the Re(0001) substrate. The distinct breaks especially in the Ag intensity–coverage relation can be correlated with the deposition of one, two, and three Ag monolayers, and therefore suggest a layer-by-layer growth mode (Frank–van der Merwe growth mechanism) with the formation of predominantly flat Ag layers. Just this growth mode has already become apparent in our previous STM study [5].

Table 1
Binding energies, kinetic energies, and inelastic mean free paths of photoelectrons excited from Ag or Re by Al Kα radiation [45]

Core level	Binding energy (eV)	Kinetic energy (eV)	Inelastic mean free path (Å)
Ag $3d_{5/2}$	367.9	1118.7	17.1
Ag $3d_{3/2}$	373.9	1112.7	17.0
Re $4f_{7/2}$	40.1	1446.5	20.7
Re $4f_{5/2}$	42.5	1444.1	20.7
Re $4d_{5/2}$	258.8	1227.8	18.3
Re $4d_{3/2}$	272.6	1214.0	18.1
Re $4p_{3/2}$	445.1	1041.5	16.2
Re $4p_{1/2}$	517.7	968.9	15.3
Re 4s	623.5	863.1	14.1

3.3. *Work function change* ($\Delta\Phi$) *measurements*

In the $\Delta\Phi$ experiments (performed with the Kelvin method) we paid particular attention to temperature and annealing effects. We measured the work function change of the Re surface after each deposition step. The necessary readjustment of the sample in front of the Knudsen cell and the Kelvin reference electrode, respectively, produced a somewhat larger error (± 20 meV) in the individual measurement than otherwise achievable with the Kelvin method (± 5 meV). To minimize this effect, we always prepared a fresh Ag film after each $\Delta\Phi$ measurement; no cumulative deposition was performed. One series (triangles) refers to a surface temperature of 300 K, the other series (circles) to 740 K. The $\Delta\Phi$ values of both series are plotted against the deposition time as displayed in Fig. 10. The constant flux conditions and the Θ-independent condensation coefficient make the abscissa entirely equivalent to a coverage scale. Again, we have marked the filling of the first and second monolayer, respectively, by thin vertical lines, based on the TDS coverage calibration. Triangles refer to room temperature, circles to high-temperature films. The general $\Delta\Phi$ behavior of the Ag films is fairly similar: we find a strong initial decrease of F of 600–700 meV as the first monolayer is populated, followed by another (but much smaller) decrease of 50–100 meV during filling of the second Ag monolayer. Still higher Ag coverages lead to a slight re-increase of $\Delta\Phi$ by some 10 meV, until a final $\Delta\Phi$ of -700 meV is reached. The influence of the deposition temperature is manifest especially during the formation of the first monolayer. Here, the decrease $d\Delta\Phi/dt$ ($\triangleq d\Delta\Phi/d\Theta$) is steeper for the 740 K film, and its $\Delta\Phi$ values are generally somewhat higher until the two curves merge again as the second monolayer is completed.

4. Discussion

The results presented in the foregoing section revealed several details about the physical and

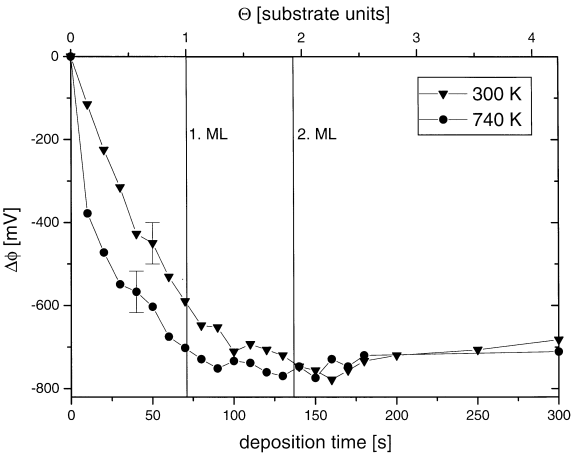

Fig. 10. Dependence of the Ag-induced work function change of a Re(0001) surface on the deposition time for two different temperatures. Using the monolayer calibration of Fig. 9, the time scale can easily be converted to a coverage (Θ) scale. Triangles refer to data points obtained for 300 K, circles to the 740 K (HT) data. Vertical lines mark the completion of the first and second monolayer, respectively. See text for further details.

chemical interaction of Ag with an Re(0001) surface. In our discussion of these features, we will focus (i) on the energetics of the desorption process in the presence of lateral Ag–Ag interactions, (ii) on the coverages associated with the individual layers, and (iii) on the growth mode, which can be deduced from the coverage-dependent XPS measurements. Thereafter, a few points concerning the "chemical" interaction between Ag and Re will be added.

The detailed analysis of the thermal desorption spectra revealed strongly coverage-dependent activation energies for desorption. They amount to merely 245 kJ mol^{-1} at low Ag surface concentrations (up to 10–15% lower than the heat of sublimation of bulk Ag of $\approx$270 kJ mol^{-1}), rise almost linearly with the Ag coverage and reach a plateau of 293 kJ mol^{-1} at medium and high Ag concentrations within the first monolayer. The reason for this behavior is, as mentioned above and discussed below, attractive lateral Ag–Ag interactions. We regard the 293 kJ mol^{-1} as characteristic of the Ag–Re interaction within the first monolayer and find this number a little higher (by $\approx$6.5%) than the heat of sublimation ΔH_{sub} of silver. This may be interpreted as evidence of a (small) "extra" interaction energy between Ag and Re. That such "extra energy" must indeed be quite small, is expected from a comparison of the Pauling electronegativities of Ag and Re, which are identical ($x=1.9$ [46]), so that a strong electronic interaction with noticeable transfer of charge appears unlikely. We shall take up this matter again when we discuss the work function properties of our interaction system.

Further support for the correctness of the evaluation of the desorption parameters is given by TD spectra simulated according to the Polanyi–Wigner equation (Eq. (1)). With the values taken from the complete analysis (cf. Section 3.1), i.e. $\nu=1.5\times10^{14}$ s^{-1}, $E^*_{des}=290$ kJ mol^{-1}, and $\beta=2.5$ K s^{-1}. TD spectra were simulated for several initial coverages ($\Theta=0.1$, 0.2, …, 0.9). In a Θ range of ±0.15 ML the desorption order was mathematically changed from 0 to 1 by a symmetric function as soon as the residual coverage became lower than 0.3 ML. The result of this simulation is shown in Fig. 11.

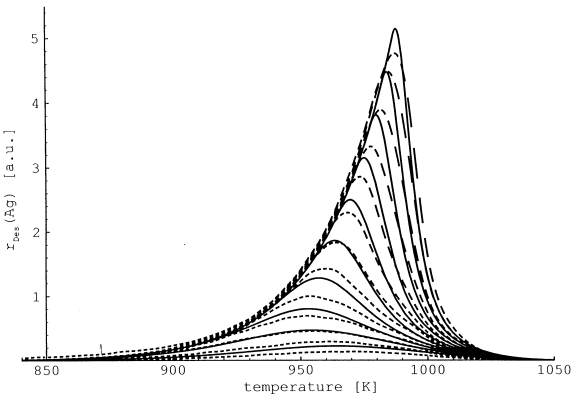

Fig. 11. Simulated (solid curve) and experimental (dashed curves) TD spectra up to $\Theta=1$ ML based on Eq. (1). The parameters $\nu=1.5\times10$ s^{-1}, $E^*_{des}=290$ kJ mol^{-1}, and $\beta=2.5$ K s^{-1} were taken from the evaluation of the TD spectra, cf. Fig. 6.

Solid lines represent the simulated data, and dashed lines the experimental data. There is a surprisingly good correspondence between the two data sets. It could be conjectured that the range of matching parameters for simulation of TD spectra is quite large and that good agreement between calculated and measured spectra can be achieved with physically unreasonable parameters, but we emphasize that even tiny variations of the chosen parameters (<5%) rendered the fit between the data sets significantly worse. Taking into account that also the variation of the reaction order at low coverages is entirely reproduced by our simple model, the idea of desorption of Ag atoms from a 2D phase equilibrium in a zero-order rate process seems quite likely.

For the multilayer range, the activation energy for desorption turns out to be practically identical with the heat of sublimation of bulk silver, namely 273 kJ mol^{-1}. No "extra" energy shows up, and we may take this result, especially in conjunction with the observation that the Ag-induced work function change has reached the bulk Ag(111) value after deposition of two to three Ag monolayers, as evidence that the electronic (and, hence, the chemical) properties of the film are those of bulk silver. In other words, the interfacial modification of the Ag film is confined to the coverage range $0<\Theta_{Ag}<2$ ML.

In order to illustrate the specific energetic behavior of the first Ag monolayer on Re(0001) it is worthwhile to compare the desorption energy and its coverage dependence with the same quantities reported in the literature for similar systems. Combined $\Delta\Phi$ and TPD measurements on the deposition of silver films on refractory metal surface were, to a great extent, carried out in the laboratories of Bauer and Kolaczkiewicz, and we rely in particular on their comprehensive data body for metal-on-metal interaction as determined from combined TD and $\Delta\Phi$ measurements. We refer especially to reports dealing with Ag on tungsten [18,20,22,47,48] and molybdenum surfaces [24,25] with their very accurate determination of the coverage dependences of the activation energy for desorption. Another valuable source of information especially about the Ag (and Cu) interaction with the Ru(0001) surface (which, as an hcp metal, resembles the Re(0001) surface even more) arises from the various studies performed in the laboratory of Wandelt [9,16,49–52].

It is thereby established that the coverage dependence of the activation energy of noble metals desorption from low-index surfaces of refractory metals exhibits a remarkable trend: with the atomically smooth (densely packed) bcc (110) surfaces of W and Mo, E^*_{des} starts from a relatively low level at very low coverages and rises strongly with Θ up to medium coverages. The rather more open (100) and (111) surfaces, on the other hand, show just the reverse behavior, namely a decrease of E^*_{des} with Θ and the stabilization on a lower level in the medium coverage range [18]. An exception to this rule is the Ag/W(211) system, where a moderate initial increase of E^*_{des} with Θ is reported in the submonolayer coverage range [20]. This peculiar behavior may be attributed to the strong anisotropy of the bcc (211) surface which induces special lateral Ag–Ag interactions in one direction, but may screen these interactions in the perpendicular direction. A comparison of our results for Ag/Re(0001) with Niemantsverdriet's results for the Ag/Ru(0001) system [16] proves to be particularly revealing. The basal Re(0001) plane with its hexagonal symmetry is also very smooth on the atomic scale, the average corrugation amplitude being only 0.1 Å [53]. The Ag/Re(0001) system follows exactly the aforementioned trend in that it exhibits an initial value for $E^*_{des,0}$ of merely 250 kJ mol^{-1} (2.59 eV at^{-1}) which rises, because of attractive lateral interactions, to $E^*_{des} = 290$ kJ mol^{-1} (3.00 eV at^{-1}) at medium coverages, an increase of 12%. Two points deserve attention here, the absolute value of the characteristic energy for Ag desorption from the monolayer, E^*_{des} and the initial rise, $E^*_{des} - E^*_{des,0}$ (which reflects the strength of the Ag–Ag interactions).

For Ag on W(110), $E^*_{des} = 342.5$ kJ mol^{-1} (3.55 eV at^{-1}) and $E^*_{des} - E^*_{des,0} = 72.4$ kJ mol^{-1} (0.75 eV at^{-1}) [22], while for Mo(110) the same quantities are 300 kJ mol^{-1} (3.11 eV at^{-1}) and 78 kJ mol^{-1} (0.81 eV at^{-1}), respectively [24,25]. Turning to the literature data for silver desorption from Ru(0001) [16,49–52], we emphasize the close correspondence between the energetic behavior of this system with that of our system: the observation of an initial increase of the activation energy for desorption as well as the absolute energy values, namely $E^*_{des,0}$ and E^*_{des}, which agree within 5 kJ mol^{-1}, are features of both systems. For vanishing Ag coverages $E^*_{des,0} \approx 250$ kJ mol^{-1} while $E^*_{des} \approx 300$ kJ mol^{-1}, leading to $E^*_{des} - E^*_{des,0} \approx 50$ kJ mol^{-1}. In addition, a first-order rate process was observed for $\Theta < 0.5$ ML and interpreted as indicative of attractive lateral interactions. As already emphasized in early reports about the interaction between Ag and Au with the (100) and (110) planes of W [48] the properties of these systems depend mainly on the substrate geometry and less on the adsorbate. It is therefore not surprising that the Ag-on-Ru(0001) and Ag-on-Re(0001) systems behave almost identically. This close similarity pertains also to the issue of the 2D phase equilibrium which was also reported for Ag/Ru(0001) [52] and other metal-on-metal systems as various detailed desorption and work function studies revealed [44,49,51–57]. For the Ag-on-Re(0001) system, we could evaluate part of the two-dimensional phase diagram of the 2D solid→2D gas transition, according to a procedure suggested by Nagai et al. [58,59]. More details will be communicated in a forthcoming publication [43].

While lateral interactions determine the morphology of the Ag layer in the submonolayer range

the situation changes dramatically as the first monolayer saturates. We know from our STM study that this first monolayer is pseudomorphic and under the influence of a high strain which can be relieved as soon as the second and third layers begin to form [5]. This (essentially microscopic) property of a "buried" interface invisible with STM measurements is accessible from our thermal desorption spectra, especially in their "layer-plot" representation, cf. Fig. 4. The high strain induced by the misfit of 4.6% in the pseudomorphic first monolayer is partly accommodated by the uniaxial expansion in the second layer. We interpret the distinct break in the plot of Fig. 5 in terms of a "reconstructed" bilayer. The first layer coverage is continuously lowered by up to $\approx 5\%$ during growth of the second layer. The completed bilayer therefore contains 10% fewer atoms than a hypothetical pseudomorphic bilayer. Further support for this interpretation is provided in Fig. 4 by the position of the minimum between the desorptive second- and third-layer contributions. It is located at $\Theta =$ 1.9 ML. The filling of the uniaxially expanded first and second monolayers is indicated by the vertical lines. That this physical relation between the first and second monolayers is indeed relevant information (which is intimately correlated with the layer misfit) is demonstrated by the Cu-on-Re(0001) system [55]. Here, a discontinuity of the shift of the first-layer minimum does not occur and the first- and second-layer maxima appear at similar coverage increments $\Delta\Theta$, the reason being the negative misfit of -7.6% between Cu and Re. In this system the coverage increment between the maxima of the first and second layer steps is simply 1. Quite generally, a bilayer reconstruction is not uncommon in metal-on-metal growth as investigations of the systems Cu/W(110) [60], Ag/W(110) [61–63], and Cu/Ru(0001) [13] show.

For higher coverages, our previous STM and LEED investigation [5] revealed the formation of fairly regular misfit dislocation domains in the third and fourth layer of the HT films, but the overall orientation of the Ag crystallites was (111). Here, the monolayer "population density" has almost reached the value characteristic of an Ag(111) surface, and a clear layer-by-layer growth has occurred. (This is evident also from the XP spectra, cf. Fig. 9.) Layer growth is regularly observed for Ag deposition on smooth (i.e. closely packed) transition metal surfaces. We refer to respective publications by Kern and his collaborators [60–63], who investigated the Ag-on-Pt(111) system by means of STM techniques and found, in many respects, similar growth features as we did with Ag films on the Re(0001) surface.

Whether or not the relaxation processes of the third layer will have an effect on the relaxation of the bilayer underneath cannot be deduced from our TPD measurements. From our previous STM investigations [5] we have, however, clear hints in this direction, because the corrugation caused by the uniaxially expanded first bilayer can no longer be seen in the STM images of the third layer.

Turning to a discussion of the work function changes, we have to consider both (i) the coverage dependence of $\Delta\Phi$ (at fixed temperature) and (ii) the temperature dependence of each individual $\Delta\Phi(\Theta)$ curve. Starting with (i) we note that the steep initial decrease of the 300 K curve, cf. Fig. 10, is followed by a shallow minimum near the monolayer and a slight re-increase of $\Delta\Phi$ as the second layer grows on top. If we neglect any kind of site exchange between Ag and Re, the experimentally measured decrease of $\Delta\Phi$ would indicate a slight positive polarization (δ^+) of the Ag adatoms, probably caused by a small transfer of electronic charge to the Re substrate. Then the $\Delta\Phi$ minimum at higher coverages could be due to depolarization of the interacting Ag dipoles. This principal $\Delta\Phi(\Theta)$ behavior is commonly observed in metal-on-metal adsorption systems including alkali-metal adsorption [64,65], and Cu, Ag, and Au films on, e.g. W or Mo surfaces [22,26,48]. We recall that our STM study [5] revealed the build-up of a pseudomorphic first Ag monolayer without any buckling. From a mere geometric point of view the respective Ag atoms can only be accommodated in a flat layer on the Re(0001) surface if the diameter of the Ag atoms shrinks by $\approx 5\%$ to overcome the positive lattice misfit. This "shrinkage" could be accomplished by the partial charge transfer to the substrate. With regard to the sign of the work function change, it is clear from the different chemical potentials of the electrons in the Re and Ag bulk (and hence the different positions of the

Fermi levels of Re and Ag) that a finite work function decrease must finally arise if the metal with the higher work function becomes covered by a film of the metal with the lower work function. Taking the work function of the clean Re(0001) surface (determined from UV photoemission experiments) as 5.4 eV [66] and our measured difference of -0.7 eV, we obtain an absolute work function of $\Phi = 4.7$ eV for the ≈ 4 ML Ag film. This agrees very well with the work function of the clean Ag(111)surface, $\Phi_{Ag(111)} = 4.74$ eV [67] and indicates that the electronic properties of the surface of a ≈ 4 ML film are already very close to what one would expect for the (111) surface of a bulk Ag crystal. The same conclusion was reached by TPD, LEED, and STM measurements.

Finally, with regard to the temperature dependence of the $\Delta\Phi(\Theta)$ function, a consideration of the individual dipole moments associated with the Ag atoms will be added. Adatoms located in an island, at the edge of an island, or delocalized as surface gas atoms (monomers, dimers, or trimers) will exhibit (slightly) different dipole moments, owing to their different local bonding situation. These differences should show up in sufficiently accurate $\Delta\Phi$ measurements, as was, for example, shown by Kolaczkiewicz for the Ag-on-W(110) and Ag-on-Mo(110) systems [47,54] and by Nohlen et al. [52] for the Ag-on-Ru(0001) system. Generally, the temperature-dependent distribution of the adatoms within the first layer will also make the work function change temperature dependent. If we associate higher dipole moments with isolated Ag atoms compared with Ag atoms bound in the 2D islands, a given number of Ag atoms should produce a greater work function change if they exist in the 2D gas phase (which is the case at elevated temperatures) but a smaller $\Delta\Phi$ if they are condensed in solid islands, i.e. at lower temperatures. This is just what Fig. 11 reveals, namely, a steeper initial decrease of $\Delta\Phi$ with coverage for the HT films, compared with the 300 K films. Unfortunately, the fairly poor accuracy of our $\Delta\Phi$ measurement does not reveal further details of the experimental $\Delta\Phi(\Theta)$ curves, in contrast to the work by Nohlen et al. [52] who were able to record work function changes continuously using a pendulum device based on a suggestion by Hölzl and Schrammen [68].

5. Conclusions

In summary, we find very satisfactory correspondence between the previously published STM and LEED data and the TDS, XPS, and $\Delta\Phi$ results reported in this work, and have extracted valuable energetic information which allows conclusions about the structure and dispersion of the Ag adatoms at temperatures close to the thermal desorption. Silver on Re(0001) grows pseudomorphically in the first layer, but rearranges in the second and third layers and then forms large islands with (111) orientation; the growth mode is layer-by-layer. Accurate TDS experiments revealed the structural rearrangement of the first layer during growth of the second layer. In addition to the strong enthalpy of condensation of Ag vapor on the Re surface we find a very minor chemical Ag–Re interaction. The activation energy of desorption increases strongly with coverage as a result of attractive Ag–Ag interactions; at sufficiently high temperatures, a two-dimensional phase equilibrium can be established, and we argue that desorption of Ag occurs from the 2D gas rather than from the 2D condensed phase.

Acknowledgements

We gratefully acknowledge technical help of R. Cames and K. Schubert and thank S. Schroeder for critical reading of the manuscript. This work has been supported by the Deutsche Forschungsgemeinschaft through SFB 290.

References

[1] L.I. Maissel, R. Glang (Eds.), Handbook of Thin Film Technology, McGraw-Hill, New York, 1970.
[2] See, for example: P. Wissmann (Ed.), Thin Metal Films and Gas Chemisorption, Studies in Surface Science and Catalysis, vol. 32, Elsevier, Amsterdam, 1987.
[3] M. Haruta, Catal. Today 36 (1997) 153.

[4] P. Claus, in: G.A. Somorjai, J.M. Thomas (Eds.), Topics Catalysis, Fine Chemical Catalysis, vol. II, in press.
[5] M. Parschau, D. Schlatterbeck, K. Christmann, Surf. Sci. 376 (1997) 133.
[6] M. Hansen, Constitution of Binary Alloys, McGraw-Hill, New York, 1958.
[7] K. Christmann, G. Ertl, H. Shimizu, J. Catal. 61 (1980) 397 (Cu/Ru(0001)).
[8] K. Christmann, G. Ertl, H. Shimizu, J. Catal. 61 (1980) 412 (Cu/Ru(0001)).
[9] A. Jablonski, S. Eder, K. Wandelt, Appl. Surf. Sci. 22/23 (1985) 305 (Ag/Ru(0001)).
[10] G. Pötschke, J. Schröder, C. Günther, R.Q. Hwang, R.J. Behm, Surf. Sci. 252 (1991) 592 (Cu, Au/Ru(0001)).
[11] R.Q. Hwang, J. Schröder, C. Günther, R.J. Behm, Phys. Rev. Lett. 67 (1991) 3279 (Cu, Au/Ru(0001)).
[12] R.Q. Hwang, C. Günther, J. Schröder, S. Günther, E. Kopatzki, R.J. Behm, J. Vac. Sci. Technol. A 10 (1992) 1970 (Cu, Au/Ru(0001)).
[13] C. Günther, J. Vrijmoeth, R.Q. Hwang, R.J. Behm, Phys. Rev. Lett. 74 (1995) 754 (Cu, Au/Ru(0001)).
[14] R.Q. Hwang, Phys. Rev. Lett. 76 (1996) 4757 (Co, Ag/Ru(0001)).
[15] S.D. Ruebush, R.E. Couch, S. Thevuthasan, Z. Whang, C.S. Fadley, Surf. Sci. 387 (1997) L1041 (Cu/Ru(0001)).
[16] J.W. Niemantsverdriet, P. Dolle, K. Markert, K. Wandelt, J. Vac. Sci. Technol. A 5 (1987) 875 (Ag/Ru(0001)).
[17] M. Stindtmann, M. Farle, T.S. Rahman, L. Benabid, K. Baberschke, Surf. Sci. 381 (1997) 12 (Ni/Re(0001)).
[18] E. Bauer, F. Bonczek, H. Poppa, G. Todd, Surf. Sci. 53 (1975) 87.
[19] E. Bauer, H. Poppa, G. Todd, F. Bonczek, J. Appl. Phys. 45 (1974) 5164.
[20] J. Kolaczkiewicz, E. Bauer, Surf. Sci. 144 (1984) 477.
[21] J. Kolaczkiewicz, E. Bauer, Surf. Sci. 151 (1985) 333.
[22] J. Kolaczkiewicz, E. Bauer, Surf. Sci. 160 (1985) 1.
[23] J. Kolaczkiewicz, E. Bauer, Surf. Sci. 175 (1986) 508.
[24] M. Paunov, E. Bauer, Appl. Phys. A 44 (1987) 201.
[25] M. Paunov, E. Bauer, Surf. Sci. 188 (1987) 123.
[26] J. Kolaczkiewicz, Surf. Sci. 200 (1988) 335.
[27] A. Pavlovska, H. Steffen, E. Bauer, Surf. Sci. 195 (1988) 207.
[28] M. Tikhov, E. Bauer, Surf. Sci. 232 (1990) 73.
[29] H. Knoppe, E. Bauer, Phys. Rev. B 48 (1993) 5621.
[30] M.W. Roberts, C.S. McKee, Chemistry of the Metal–Gas Interface, Clarendon Press, Oxford, 1978, p. 272 ff.
[31] D.A. King, Surf. Sci. 47 (1975) 384.
[32] C.T. Campbell, Annu. Rev. Phys. Chem. 41 (1990) 775.
[33] J.A. Rodiguez, R.A. Campbell, D.W. Goodman, J. Vac. Sci. Technol. A 10 (1992) 2540.
[34] J.W. He, D.W. Goodman, J. Phys. Chem. 94 (1990) 1496.
[35] J.W. He, D.W. Goodman, J. Phys. Chem. 94 (1990) 1502.
[36] K. Nagai, Surf. Sci. 176 (1986) 193.
[37] A.M. de Jong, J.W. Niemantsverdriet, Surf. Sci. 223 (1989) 355.
[38] T.S. Wittrig, D.E. Ibbotson, W.H. Weinberg, Appl. Surf. Sci. 4 (1980) 234.
[39] I. Barin, O. Knacke, Thermochemical Properties of Inorganic Substances, Springer, Berlin, 1973.
[40] H. Schlichting, D. Menzel, Surf. Sci. 272 (1992) 27.
[41] G. Lauth, T. Solomun, W. Hirschwald, K. Christmann, Surf. Sci. 210 (1989) 201.
[42] K. Christmann, Introduction to Surface Physical Chemistry, Steinkopff, Darmstadt 1991, p. 70 ff., and Refs. therein.
[43] R. Wagner, D. Schlatterbeck, K. Christmann, to be published.
[44] E. Bauer, Appl. Phys. A 51 (1990) 71.
[45] S. Tanuma, C.J. Powell, D.R. Penn, Surf. Interf. Anal. 17 (1993) 927.
[46] L. Pauling, Die Natur der chemischen Bindung, 2nd ed., Verlag Chemie, Weinheim, 1964.
[47] J. Kolaczkiewicz, Surf. Sci. 84 (1979) 475.
[48] E. Bauer, H. Poppa, G. Todd, P.R. Davis, J. Appl. Phys. 48 (1977) 3773.
[49] B. Konrad, F.J. Himpsel, W. Steinmann, K. Wandelt, Proceedings ER-LEED 85, 1985, p. 109.
[50] M. Schick, J. Schäfer, K. Kalki, G. Ceballos, P. Reinhard, H. Hoffschulz, K. Wandelt, Surf. Sci. 287/288 (1993) 960.
[51] J. Schäfer, P. Reinhard, H. Hoffschulz, K. Wandelt, Surf. Sci. 313 (1994) 83.
[52] M. Nohlen, M. Schmidt, H. Wolter, K. Wandelt, Surf. Sci. 337 (1995) 294.
[53] M. Parschau, K. Christmann, Ber. Bunsenges. Phys. Chem. 95 (1996) 1376.
[54] J. Kolaczkiewicz, Surf. Sci. 231 (1990) 103.
[55] R. Wagner, D. Schlatterbeck, K. Christmann, Verhandl. Dtsch. Physik. Ges. 1998 Regensburg, (O-11.22), to be published.
[56] J. Kolaczkiewicz, E. Bauer, Phys. Rev. Lett. 54 (1985) 574.
[57] J. Kolaczkiewicz, E. Bauer, Surf. Sci. 155 (1985) 700.
[58] K. Nagai, T. Shibanuba, M. Hashimoto, Surf. Sci. 145 (1984) L459.
[59] K. Nagai, Phys. Rev. Lett. 54 (1985) 2159.
[60] E. Bauer, Appl. Surf. Sci. 11/12 (1982) 479.
[61] H. Röder, H. Brune, J.-P. Bucher, K. Kern, Surf. Sci. 298 (1993) 121.
[62] H. Brune, H. Röder, C. Borragno, K. Kern, Phys. Rev. B 49 (1994) 2997.
[63] K. Bromann, H. Brune, H. Röder, K. Kern, Phys. Rev. Lett. 75 (1995) 677.
[64] J. Hölzl, L. Fritsche, Surf. Sci. 247 (1991) 226.
[65] A. Neumann, S.L.M. Schroeder, K. Christmann, Phys. Rev. B 51 (1995) 17007.
[66] K. Christmann, unpublished.
[67] J. Hölzl, F.K. Schulte, Springer Tracts in Modern Physics, vol. 85, Springer, Berlin, 1979.
[68] P. Schrammen, J. Hölzl, Surf. Sci. 130 (1983) 203 and Refs. cited therein.